J. Astrophys. Astr. (2022)43:85
https://doi.org/10.1007/s12036-022-09861-4

ACTIVE GALACTIC NUCLEI

Jets from active galactic nuclei

KULINDER PAL SINGH[1,2,]

[1]Department of Physical Sciences, Indian Institute of Science Education and Research Mohali, Sector 81, SAS Nagar, Mohali 140306, India.
[2]Department of Astronomy and Astrophysics, Tata Institute of Fundamental Research, Homi Bhabha Road, Mumbai 400005, India.
E-mail: kpsinghx52@gmail.com

MS received 30 December 2021; accepted 9 May 2022

Abstract. In this article, first the author present a short historical introduction to the discovery of extra-galactic jets in active galactic nuclei (AGN), followed by a brief overview of their observational properties which lead to their various classifications and a unification scheme based on the viewing geometry of jets in the AGN. The author largely focus on the studies of multi-wavelength emissions and modeling of spectral energy distribution of AGN, which are dominated by emission from jets, namely, blazars. The author present a few new results from the studies of a few blazars based mostly on observations with the AstroSat. The author ends with an overview of the role played by the radio jets in clusters of galaxies in creating various interesting features in the hot gas, and feedback and regulation of heating and cooling in the cores of the hot gas.

Keywords. Active galactic nuclei: jets—multi-wavelength, X-rays—clusters of galaxies—radio, X-rays.

1. Introduction

The first extragalactic jet—a collimated linear emission in optical, was discovered in 1918 by Herber Curtis in a photograph taken at the Lick Observatory in USA of a giant elliptical galaxy, Messier 87 (M87) in the Virgo constellation. M87, also known as NGC 4486, is at a distance of $\sim$53 million light years (Ly) and has a jet of energetic plasma originating at the core and extending at least 4900 Ly. A modern day image taken with the digital cameras aboard the Hubble Space Telescope is shown in Figure 1, clearly showing a blue colored plasma jet.

This discovery was followed by the observation of an unusual spectrum at the center of some galaxies with very bright centers in 1943 by Carl Seyfert. These galaxies are also distinguished themselves by having a very bright star-like nucleus, but with non-stellar spectrum (very broad-emission lines) (Seyfert 1943). The nuclear emission in many cases exceeds that from all stars in a normal galaxy by 1–5 orders of magnitude. A modern day image of one such galaxy, NGC 4593, taken with AstroSat ultra-violet imaging telescope (UVIT) (Singh *et al.* 2014; Tandon *et al.* 2017) camera in a broad filter centered at 245 nm is shown in Figure 2 (top panel). Subsequently, the nuclear emission from such galaxies have been found to show large and rapid variability across the electromagnetic spectrum from radio to γ-rays. An example of such rapid variability seen from the nucleus of NGC 4593 in soft X-rays with the AstroSat soft X-ray telescope (SXT) (Singh *et al.* 2016, 2017) is shown in Figure 2 (bottom panel). With a doubling time as short as $\sim$10 ks leads to a very compact size, $\sim 10^{14-15}$ cm, for the nuclear region, based on simple light travel time arguments. This combined with enormous luminosity implies a very large mass: ($>5 \times 10^5$) the mass of the Sun, in a small nuclear region. Thus has born the notion of a putative super-massive black hole in each of these powerful nuclei of galaxies, also collectively called active galactic nuclei (AGN). Today, we believe that all galaxies harbor an AGN. Observations have shown that the masses of

This article is part of the Special Issue on "Astrophysical Jets and Observational Facilities: A National Perspective."

Published online: 11 November 2022

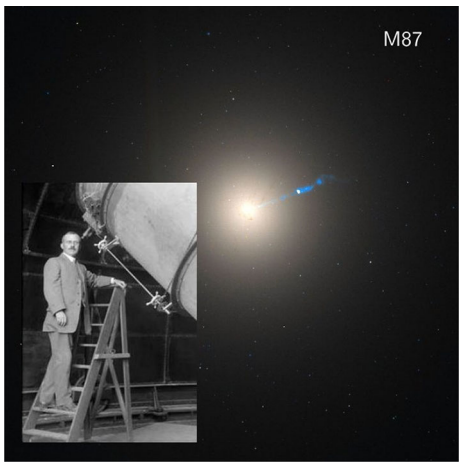

Figure 1. A composite image of M87 from observations in visible and infrared light as observed by the Hubble Space Telescope with H. Curtis in the foreground (Credits: NASA/CXO and Lick Observatory).

supermassive black holes in the nuclei of galaxies correlate with the velocity dispersions (σ) of their bulges, $M_{\rm SMBH} \propto \sigma^{\alpha}$, where $\alpha = 4.8 \pm 0.5$ (Ferrarese & Merritt 2000).

In 1950s, hundreds of discrete radio sources were discovered and published in the third Cambridge catalog (3C), while optical astronomers looked for their counterparts (Shields 1999). Definite identifications of two radio sources, 3C48 and 3C273, were made in 1963 with star-like objects at the location of the radio source. Their optical spectra were obtained and found to contain many unknown broad emission lines at a very high redshift (Schmidt 1963). Large redshift of 3C273 implied that the object was much more luminous than any galaxy. Historical records of 3C273 also showed that it was variable on yearly timescales, implying that its light was emitted from a very compact region <1 pc size. Many such objects were discovered and dubbed as quasars (quasi stellar radio sources), while similar objects discovered through optical spectroscopy, but without any radio emission or very faint radio emission were called quasi stellar objects (QSOs).

Hazard *et al.* (1963) observed a lunar occultation of 3C273 and reported that the radio source had two components: 3C273B coinciding with a star and 3C273A at $\sim$20 arc-sec distance coinciding with a faint wisp or jet pointing away from the star. The jet can be seen clearly at many wavelengths including X-ray telescopes. An X-ray image of 3C273 and multi-wave (optical, X-ray and radio) images of only the jet in 3C273 are shown in Figure 3. The jet has

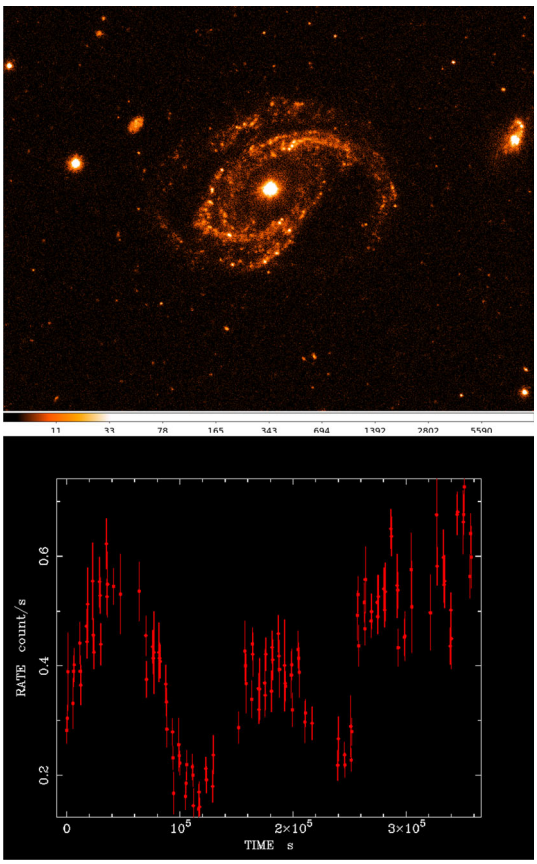

Figure 2. Seyfert galaxy: NGC 4593 as imaged in the UV (245 nm broad-band filter) with the UVIT telescope aboard AstroSat (top). The soft X-ray light curve obtained with the AstroSat SXT (Credits: G. C. Dewangan).

several knots superposed on a continuous flow. The X-ray output of the first knot in the jet is greater than that of most Seyfert galaxies. It is believed that the jet carries energy emitted by the gas that falls toward a supermassive black hole at the center of the compact object, redirected and confined by strong electromagnetic fields into a collimated jet.

1.1 *Superluminal motion*

In 1980–1990, bright radio emission in the form of jets was observed from many quasars using the very long baseline array (VLBA) of telescopes distributed globally thus, providing sub-milliarcsec to milliarcsec spatial resolution. One such example is 3C279. It was imaged several times at 22 GHz times for 10 years by Wehrle *et al.* (1996) and shown in Figure 4. Blobs of plasma emitting radio waves, most likely from shocked material, in a well-directed stream can be seen to move out of a stationary object with

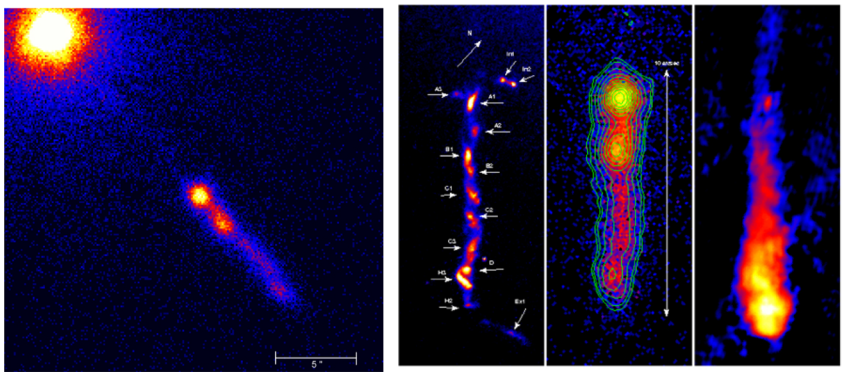

Figure 3. Left: X-ray image of 3C273 from observations with Chandra X-ray Observatory. Right: Multiwavelength: Optical (left), X-ray (center) and radio (right), views of the jet emission in 3C273 (Credits: Optical: NASA/STScI, X-ray: NASA/CXC/SAO/Marshall *et al.*, Radio: MERLIN).

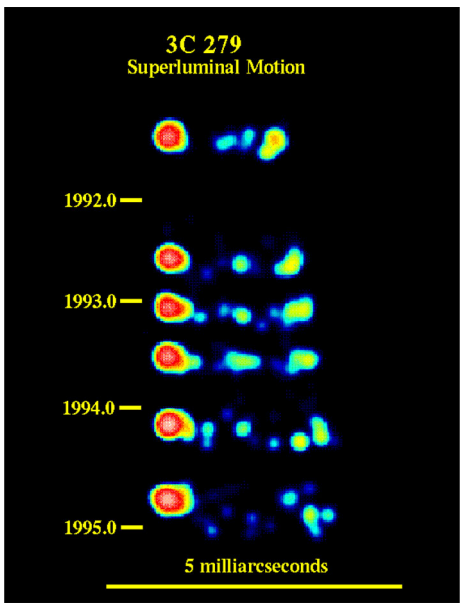

Figure 4. Superluminal jet in 3C279. Images from 22 GHz (wavelength 1.3 cm) observations with VLBA, rotated by 30° to make the jet horizontal and vertically displaced according to the date of observation. The resolution is about 0.2 milliarcsecond, corresponding to about 2 light-years at this distance (Credits: Ann Wehrle and Steve Unwin, see also Wehrle *et al.* 1996).

variable intensity. The blobs appear to move at superluminal (apparent velocity > speed of light) speed. This can been understood if the blobs of material from very distant objects in the universe (redshift of 3C279 is 0.5362 making it a very distant object) are moving at relativistic speed and are directed at very small angles to our line of sight. High levels of radio polarization of inner blobs with electric field vectors parallel to the jet direction were interpreted by Wehrle *et al.* (1996) as 'regions where the initially tangled magnetic fields have been so highly compressed that the resulting magnetic fields are perpendicular to the directed flow'.

1.2 *BL Lac types and blazars*

In 1929, a German astronomer Cuno Hoffmeister published a catalog of 354 objects which he thought as variable stars. One of these variable stars was BL Lac in the stellar constellation known as Lacerta (Lizard). The peculiar nature of BL Lac, namely, erratic variability, strong radio emission, a faint and fuzzy galaxy around it, its distance, polarization, etc., was detected in 1960–1980, making it a special class of objects named after this prototype, and later on expanded into a more general class of objects named as blazars.

Subsequently, a radio source known as PKS 2155–304, discovered as the brightest extragalactic soft X-ray source with HEAO-1 by Agrawal & Riegler (1979), and was identified as a type of blazar. This was also the target for the first light observation with the soft X-ray telescope (SXT) aboard the AstroSat on 26 October 2015. The source is highly variable in X-rays on time scales ranging from days to years. X-ray variability of PKS 2155−304 from the SXT observation is shown in Figure 5. Many blazars have been discovered and observed since 1970s and found to emit over a very broad range of electromagnetic spectrum ranging from radio to very high energy γ-rays. These objects are highly variable at all wavelengths and they dominate the γ-ray sky being monitored continuously with the *Fermi* observatory. An example of a γ-ray flare observed with the *Fermi* and followed nearly and simultaneously across all the other wavebands from X-rays to radio is shown in Figure 6.

2. Classification schemes

A classification scheme based on optical properties of all types of AGN has been provided by Blandford *et al.* (2019) in their review article and is reproduced in Table 1. The space densities of various types of AGN are also given in Table 1. AGN that are found to emit strongly in radio are also classified based on their radio properties. This scheme named them as follows: Fanaroff–Riley type 1 (FR-I) are low-power edge-darkened radio sources with luminosity $<10^{42}$ erg s^{-1}; Fanaroff-Riley type 2 (FR-I) are high-power edge-brightened radio sources with higher luminosity $>10^{42}$ erg s^{-1}; BL Lac (BLL) objects as compact radio sources with polarized optical continuum and weak or no emission lines and luminosity $<10^{42}$ erg s^{-1}; and finally flat-spectrum radio quasars (FSRQ) for compact radio sources identified with a quasar and luminosity $>10^{42}$ erg s^{-1}. The FR-I type AGN are found to be the most abundant ($\sim 10^{4.0}$ Gpc^{-3}) in the local universe, while the other types are $\sim$2–3 orders of magnitude, less abundant (Braun 2012; Ajello *et al.* 2014; Tadhunter 2016).

Many types of BLLs have been discovered based on their broad-band spectral energy distributions (SEDs), and are together known as Blazar family. The SEDs of blazars are distinguished by the presence of two broad-band humps—one peaking in the infra-red to soft X-ray energy band and the other dominating the

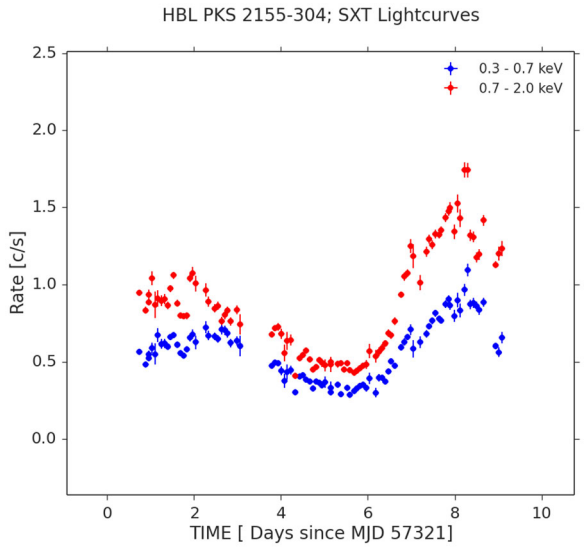

Figure 5. X-ray flare observed from PKS2155−304 with AstroSat SXT in two energy bands (Credits: S. Chandra).

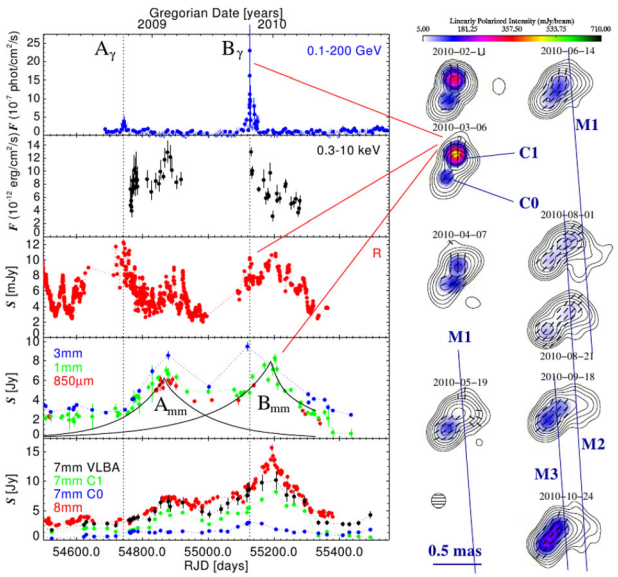

Figure 6. A γ-ray flare from OJ 287 with simultaneous X-ray, optical and radio flares (Credits: Agudo 2011).

Table 1. Classification of AGN by optical properties.

Type of AGN	Defining property	Bolometric luminosity (ergs s^{-1})	Local space density
LINER: Low ionization nuclear emission region	Weak Seyfert like galaxy	$<10^{42}$	$\sim 10^{6.5}$
Sy 2: Seyfert galaxy type 2 AGN	Narrow permitted and forbidden lines	$>10^{42}$	$\sim 10^{5.5}$
Sy 1: Seyfert galaxy type 1 AGN	Broad permitted and narrow forbidden lines	$>10^{42}$	$\sim 10^{5.0}$
QSO: Quasi-stellar object	AGN outshining the host galaxy	$>10^{45}$	$\sim 10^{2.5}$
WLRG: Weak-line radio galaxy	Radio galaxy analog to LINER	$<10^{42}$	$\sim 10^{4.0}$
NLRG: Narrow-line radio galaxy	Radio galaxy analog to Sy 2	$>10^{42}$	$\sim 10^{1.2}$
BLRG: Broad-line radio galaxy	Radio galaxy analog to Sy 1	$>10^{42}$	~ 10
Quasar: Quasi-stellar radio source	QSO with strong radio emission	$>10^{45}$	$\sim 10^{-1.5}$

Classification scheme from Blandford *et al.* (2019). Local space densities (in units of Gpc^{-3}) are from Tadhunter (2016).

γ-ray energies from MeV to TeV. The location of the humps in the energy depends on the luminosity of a blazar and thus defines another sequence of blazars as shown in Figure 7. It can be seen that both the peaks shift towards lower energies as the luminosity increases. The highest luminosity objects are the FSRQs, followed by sub categories (in the order of luminosity) of BLLs. These are LBL: Low-frequency peaked BL Lac types because of the positions of their peaks, IBL: Medium-luminosity BLLs with peaks at intermediate frequencies, HBL: Low power BLLs with peaks at very high frequencies, and finally EBLs as the low-powered extreme HBLs with their second peak in TeV band. Further attributes of these objects in the optical and their relation to the radio types described above are given in Table 2.

2.1 *AGN: a unified view*

All the main physical components in an AGN are listed in the classification schemes, and are displayed in a unified picture shown schematically in Figure 8. An accreting SMBH is at the center of each type of AGN surrounded by an accretion disk, which is too small to be resolved by present day telescopes. Accretion disks in AGN are usually optically-thick and physically-thin (Shakura & Sunyaev 1973) with temperatures in the range of $\sim 10^5$–10^6 K, thereby emitting optical and ultraviolet radiation. A corona of very hot electrons, probably heated by processes similar to that in Solar corona involving magnetic fields, is believed to exist close to and above the accretion disk. Discrete and patchy clouds exist much further out from the SMBH and are responsible for line emission from AGN, generated mainly by photo-ionization with some contribution from collisional excitation. Thick (electron density of 10^7–10^{10} cm^{-3}) clouds closer to the SMBH, emit very broad permitted recombination lines (full width at half maximum (FWHM) ≥ 3000 km s^{-1}). This region known as broad line region (BLR) exists on scales smaller than a parsec (pc) within the deep gravitational potential of SMBH, where lines are broadened due to large random velocities. The presence of BLR in an AGN is responsible for being designated as type 1—Seyferts, quasars, etc. Absence of BLR and presence of only narrow (FWHM $\sim$ 500 km s^{-1}) permitted and forbidden lines lead to type 2 designation. It is called the narrow line region (NLR), it has low density of $\sim 10^4$ cm^{-3} and extends over scales of tens to hundreds of pc. Here, the emitted lines are all narrow due to weaker gravity. An optically-thick obscuring matter (dust or electron plasma in the form of a torus) blocks the line-of-sight to the nucleus of an AGN, obscuring the BLR region. Scattered polarized light has been observed from type 2 sources, however, making the presence of torus ubiquitous. The NLR in all AGN is believed to lie above the torus. The angle of the torus to our line-of-sight is a key parameter that decides the class of an AGN. Radio loud (RL) AGN and quasars are objects with directed or relativistic jet emission. Blazars are interpreted as a subset of these radio-sources, where the

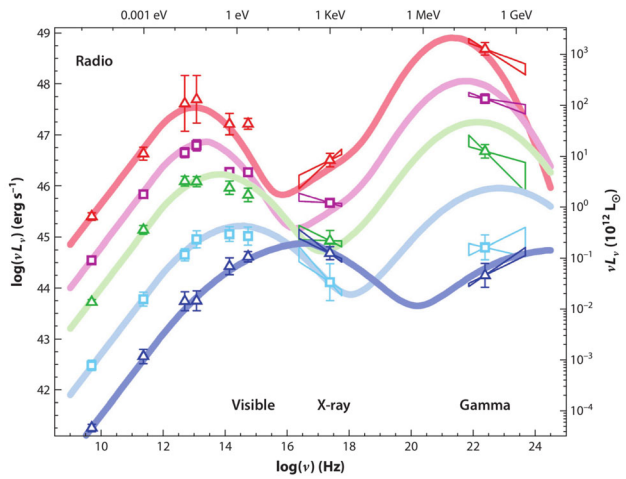

Figure 7. Blazar SED sequence based on luminosity, showing a high-powered FSRQs (red), LBL (pink), medium-luminosity IBL (green), HBL (light blue) and low-powered extreme HBL/TeV (dark blue) blazar, after (Fossati *et al.* 1998) (Credits: Blandford *et al.* 2019).

Table 2. Classification of blazars.

Type of blazar	Defining properties
EHBL	Extreme HBL with TeV emission, weak emission lines and low luminosity FR-I radio counterpart
HBL	High energy peaked BLL with weak emission lines and FR-I radio counterpart
IBL	Intermediate energy peaked BLL with weak emission lines and FR-I/II break radio counterpart
LBL	Low energy peaked BLL with weak emission lines and FR-II radio counterpart
FSRQ	Flat spectrum radio quasar with strong emission lines and FR-II radio counterpart

Classification scheme from Blandford *et al.* (2019).

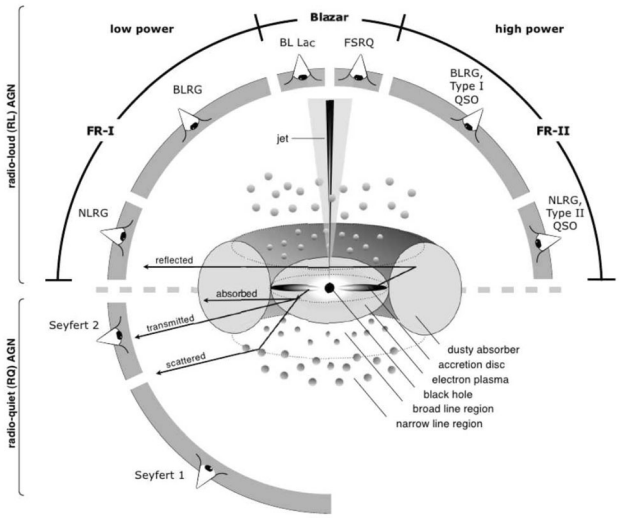

Figure 8. A unified representation of the AGN phenomenon based on the viewing angle, the presence or absence of the jet, and the power of central engine in AGN. The radio loud objects are believed to have symmetric double sided jets, but are shown here with a one-sided jet for illustration purposes (Credits: Beckmann & Shrader 2012).

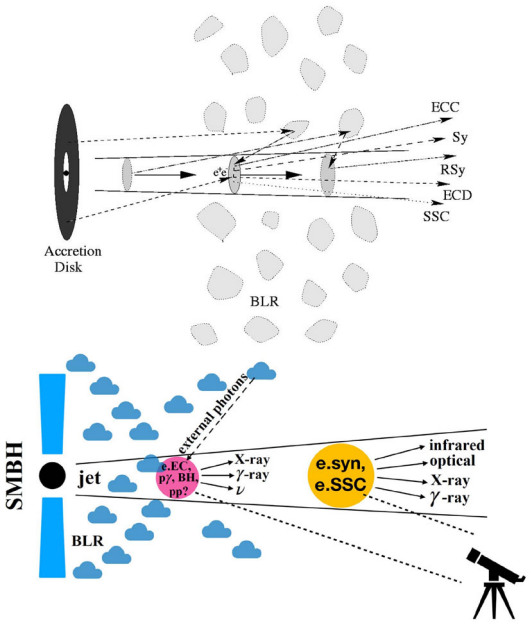

Figure 9. Top: A schematic illustration of the possible emission processes from a leptonic jet in a blazar (see the text). Credits: Bottcher (2002). Bottom: Two-zone photo-hadronic ($p\gamma$) model with one of the zones (orange) being far away from the BLR, and the other being close to or inside the BLR (Credits: Xue & Liu 2019).

relativistic jet is aligned almost along the line of sight ($<10^{\circ}$) to the observer (Urry & Padovani 1995).

3. Blazars: emission mechanisms

Very high luminosities, rapid variability and superluminal jets apparently directed at the observers are evidence that the continuum emission of blazars from radio to γ-rays is produced in very compact (<1 pc) and relativistically moving emission regions. The lower energy (radio to soft X-rays) emission component is via Syn radiation from the jet, whereas the high-energy (γ-ray) component is believed to arise through the IC scattering in two possible scenarios: leptonic and hadronic. In the leptonic scenario, highly relativistic electrons in the jet plasma boost the energy of soft photons by the IC process (Bottcher 2007). These soft photons could originate from the local synchrotron radiation within the jet producing the synchrotron self-compton (SSC) component (Maraschi *et al.* 1992; Zhang *et al.* 2012) or they could be the UV photons from the accretion disc (Dermer & Schlickeiser 1993), or the accretion disc photons reprocessed by broad-line region (BLR) clouds (Sikora *et al.* 1994) or the infrared (IR) photons from the dusty torus (Blazejowski *et al.* 2000). Some of the processes are shown in Figure 9 (top). Here, ECD refers to external comptonization of direct disk radiation, ECC is external comptonization of radiation from clouds. In addition, there can be RSy (reflected synchrotron) emission and some IR emission from circum-nuclear dust in the low energies. The location of GeV γ-ray emission region is, however, unresolved. Rapid variability observed at different wavelengths is the only way at present to resolve this issue, but requires simultaneous observations at different wavelengths. Spectral shape of the GeV emission has also been proposed as a diagnostic test for the location of the GeV emission (Cao & Wang 2013).

Since the astrophysical jets are also believed to be the sites for the injection of cosmic rays and protons in the Universe, the very high-energy emission can also originate from proton synchrotron or photon-hadronic interaction in the hadronic models (Mannheim 1993; Mucke *et al.* 2003; Bottcher *et al.* 2009). Protons with Lorentz factors of 10^9–10^{11} can generate photons with keV to TeV energies via pion production and pair production followed by synchrotron casacade processes (Mannheim & Biermann 1992). Hadronic origin of the very high energy (VHE) emission can be obtained indirectly by the observation of VHE neutrinos since lost by protons as they interact with the jet is almost equally divided into electromagnetic and

neutrinos components. The neutrinos thus produced escape the emitting region, carrying information about the protons in the jet. Both the leptonic and hadronic processes have been invoked either in a single zone (or site) or multiple (usually two) zones to explain the observed SEDs of blazars.

3.1 *One-zone model*

A simple model to understand the X-ray and γ-ray emission from a blazar is described in Kushwaha *et al.* (2013). It consists of a single zone made of a spherical region of size, R, moving down the jet at a relativistic speed, βc, with bulk Lorentz factor Γ at an angle θ with the line of sight, thus having a Doppler factor $\delta = [\Gamma(1 - \beta\cos\theta)]^{-1}$. The emission region is permeated with a tangled magnetic field B and populated by a broken power-law distribution of particles. The size can be constrained by the variability time-scale and θ estimated from very long baseline array (VLBA) studies, while the Γ is obtained from the observed superluminal velocities. Particles radiate their energy through synchrotron and SSC/EC processes. A plausible mechanism responsible for the high energy emission can then be argued by trying to fit the observed fluxes in optical, X-ray and γ-ray energies with the predicted fluxes assuming either synchrotron+SSC or synchrotron+EC or all three processes as shown in Figure 9 (bottom) from Xue & Liu (2019). The optical-UV emission is due to synchrotron process. This model was used successfully to explain the three states of a flare observed in 2009 from OJ 287 by Kushwaha *et al.* (2013) as shown in Figure 10. Kushwaha *et al.* (2013) showed that a combination of both SSC and EC mechanisms can reproduce the observed high energy spectrum and that the emission region of OJ 287 is surrounded by a warm infrared emitting region of $\sim$250 K located at a distance of $\sim$9 pc consistent with the deduction made from mmγ-ray correlation study and VLBA images by Agudo (2011). This is much further than the BLR region shown in Figure 9 (top) and is more like one of the two zones shown in Figure 9 (bottom).

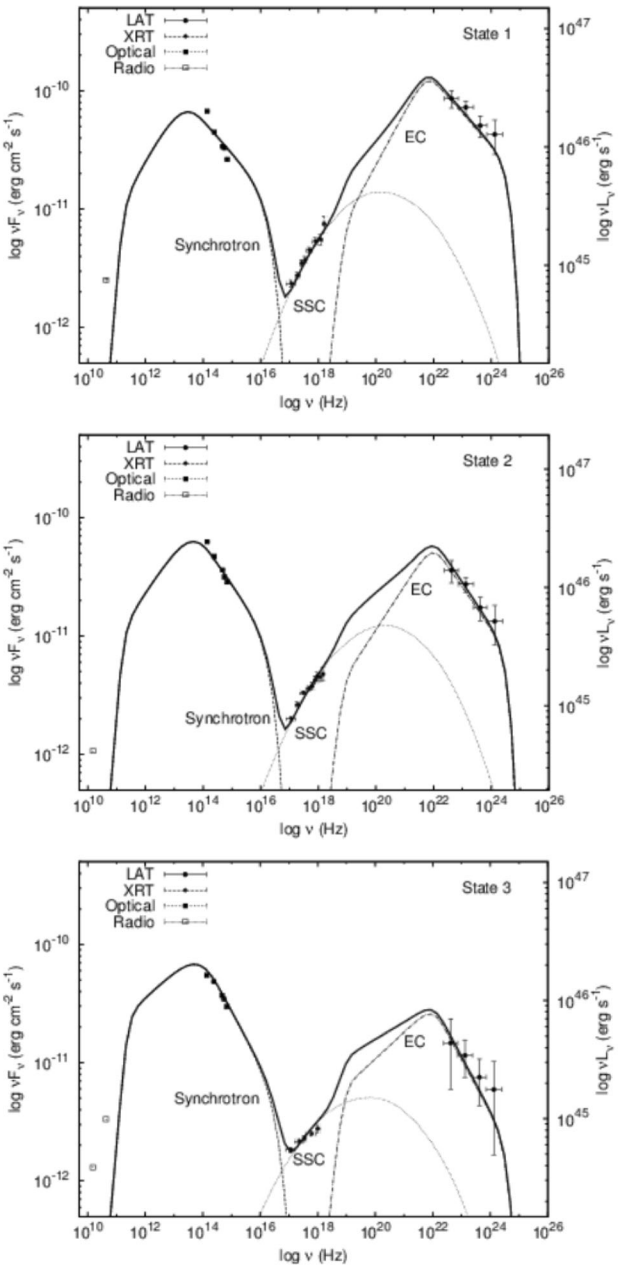

Figure 10. SED of OJ 287 during the three states of a flare in 2009 modeled with synchrotron, SSC and EC processes. The high energy emission is fitted with both SSC and EC processes. The dashed, dotted and the dash–dotted curves represent the synchrotron, SSC and EC spectral components, respectively. The solid curve is the sum of emissions from all the spectral components (Credits: Kushwaha *et al.* 2013).

3.2 *Two-zone model*

Two-zone models can have leptonic processes taking place in both the zones or a combination of leptonic processes in one zone and hadronic processes in the other. A two-zone lepto-hadronic model is shown in Figure 9 (bottom). In the model shown, photons from the BLR are assumed to lead to efficient γ-ray production (via the EC process), and also produce neutrinos by the photohadronic ($p\gamma$) process and possibly the pair-production (pp) process. The radiation from

the secondaries produced in $p\gamma$, Bethe–Heitler (BH) or pp processes can emerge in X-rays and γ-rays. This is also known as the HBL part of the SED. The low-energy (infrared to soft X-ray) synchrotron radiation from the inner zone is likely to be suppressed by the dominant Compton cooling of electrons, and therefore, more likely to emerge from the synchrotron emission of electrons from the outer zone having negligible BLR radiation. This is also known as the LBL part of the SED. The outer zone may also produce hard X-rays and γ-rays via the SSC process of accelerated electrons as described in more detail by Xue & Liu (2019).

VHE γ-ray (>100 GeV) emission detected from a well-known FSRQ, 3C279, detected with major atmospheric gamma-ray imaging Cherenkov (MAGIC) telescope required a two-zone model in which the optical emission is produced in a different region than the VHE γ-ray emission (Bottcher *et al.* 2009). Both SSC model (leptonic processes in both the zones) with an emission region far outside the BLR or a lepto-hadronic model is capable of reproducing the simultaneous X-ray-VHE γ-ray spectrum of 3C279 (Bottcher *et al.* 2009; Hayashida *et al.* 2012). In the second case, the internal synchrotron field serves as targets for $p\gamma$ pion production with a substantial contribution from external photons, e.g., from the BLR (Bottcher *et al.* 2009).

The detection of VHE neutrinos in an event known as IceCube 170922A (Collaboration 2018) and its association with a blazar, TXS 0506+056, has provided a filip to the lepto-hadronic models for the VHE emission from blazars (Gasparyan *et al.* 2022). An excess of ~ 13 neutrinos seen in the archival data taken between September 2014 and March 2015, in the direction of TXS 0506+056, has further corroborated this association (IceCube Collaboration 2018). A general simulation code, known as simulator of processes in relativistic astronomical objects (SOPRANO) has been developed by Gasparyan *et al.* (2022) to study leptonic and hadronic processes in relativistic sources, such as blazars and γ-ray bursts. SOPRANO follows the time evolution of isotropic distribution functions of protons, neutrons and the secondaries produced in hadronic processes, alongwith the evolution of photon and electron/positron distribution functions. It has been used by Gasparyan *et al.* (2022) to model the broad-band spectrum of TXS 0506+056. These observations have also opened up the possibility to perform multi-messenger studies of blazar jets.

Two-zone leptonic model are also used and found to be responsible for the SEDs during the high-activity states of OJ 287 (Kushwaha *et al.* 2018). These have also been invoked in explaining the SEDs of OJ 287 observed during three AstroSat multi-wavelength observations shown in Figure 11. This study shows the spectral evolution of the source from the time when the HBL component was ending in 2017 to its disappearance in 2018, and its revival in 2020 (Singh *et al.* 2022). Though a single-zone leptonic model is sufficient to reproduce the 2018 SED, the 2017 and 2020 SEDs also require an additional HBL-like emitting inner zone, with the observed changes in the X-ray spectrum primarily driven by the evolution of the optical-UV synchrotron spectrum (Singh *et al.* 2022).

4. FR-I and FR-II sources in hot X-ray gas

4.1 *Cavities, bubbles, filaments and shocks*

Cavities and bubbles created by radio sources, usually FR-I type, in the hot intragalactic gas or intracluster medium were first seen in the Perseus cluster core by Boehringer *et al.* (1993) using the ROSAT. Since then, many examples have been reported from observations with the Chandra X-ray Observatory. Perseus cluster, the X-ray brightest cluster in the sky, remains the best example, showing concentric ripples (Fabian *et al.* 2003, 2006) which were interpreted by the authors as 'due to sound waves generated by the expansion of the central pressure peaks associated with the repetitive blowing of bubbles'. The ripples have small amplitudes <10%, so they are very difficult to detect in fainter clusters (Graham *et al.* 2008). Outbursts from SMBH, specially when the radio sources are FR-II types with strong radio jets, where jets can transport energy and create not only buoyant bubbles, but also transfer energy to the hot gas by shocks (usually, seen as weak shock fronts with sudden change in temperatures across it) or turbulence, and produce filamentary structures in X-ray gas. An example of such features can be seen in a very deep image of M87 taken with the Chandra X-ray Observatory (Forman *et al.* 2007; Million & Werner 2010) and shown in Figure 12. The image shows the relative deviations of the surface brightness from a radially averaged surface brightness model (data-model/model) on the left and a low frequency (90 cm) radio image from Owen *et al.* (1990) on the right. One can see several features like shocked regions, arms likely driven by the central AGN in M87, an outer cavity beyond the eastern arm, a sharp edge in the eastern arm, and an outer partial ring. The eastern and

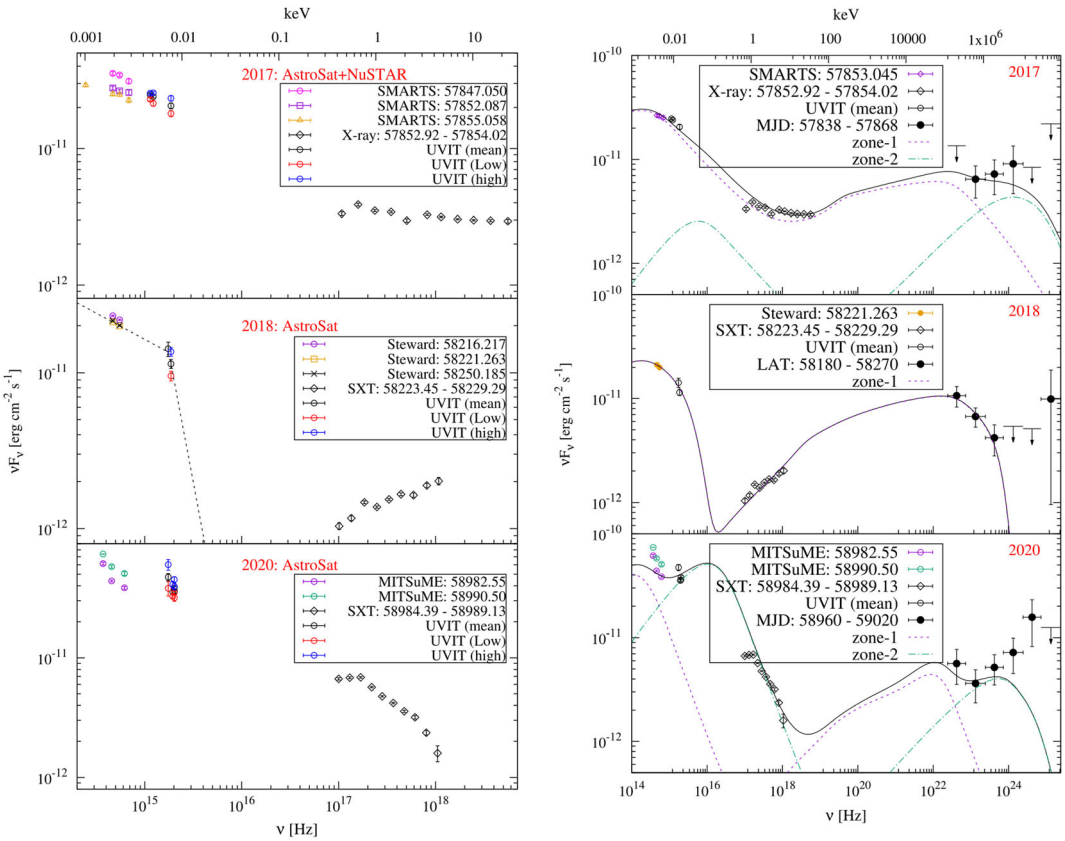

Figure 11. Left: SEDs of OJ 287 from 3 AstroSat observations using UVIT and SXT, along with contemporaneous NIR-optical data from public archives. The highest, lowest and the mean UVIT fluxes are shown in blue, red and black. Right: The SEDs extended to γ-rays and modeled using single and double zone models. The broad-band emission spectrum of the outer zone (zone-1) and the inner zone (zone-2) are shown as dashed and dotted–dashed curves, respectively, while the black curve is the sum of these two. For the 2018 data, one-zone model is sufficient to account for the SED (Credits: Singh *et al.* 2022).

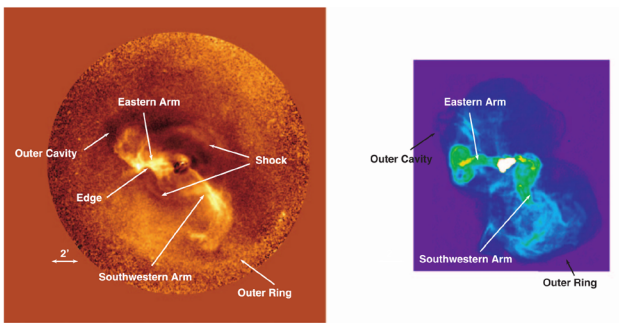

Figure 12. Left: M87 in soft X-rays (0.5–2.5 keV) showing the relative deviations of the surface brightness from a radially averaged surface brightness model (data-model/model). Point sources have been removed and substituted by a local background. Right: Radio (90 cm) image from Owen *et al.* (1990) at the same scale as the Chandra image (Credits: Forman *et al.* 2007).

southwestern arms are visible in both X-ray and radio. An outer X-ray cavity (depression) corresponds to an enhancement in the radio, and the outer bright (enhancement) X-ray ring is just beyond the edge of the large-scale radio emission. A torus like structure in the radio, at the end of the eastern arm, is connected by the arm to the center of M87. The torus and arm produce a mushroom-shaped structure (cap and stem) (Forman *et al.* 2007; Million & Werner 2010).

Double sided, almost symmetric jets of radio plasma imaged with the very large array have been seen emanating from very large elliptical galaxies and surrounded by hot X-ray emitting intergalactic gas. Two such examples are shown in Figure 13 for Cygnus A and Hercules A radio sources. Cygnus A, an FR-II radio galaxy, is in the central region of a cluster of galaxies about 760 million Ly from Earth. The jet in Cygnus A is not only immersed in the hot gas, but is also seen to emit X-rays. Radio and X-ray data also reveal 'hot spots' at a distance of 300,000 Ly from the center of the galaxy at the ends of the jet. The jet in Hercules A spans almost a million Lys. Confined low surface brightness regions or depressions in the

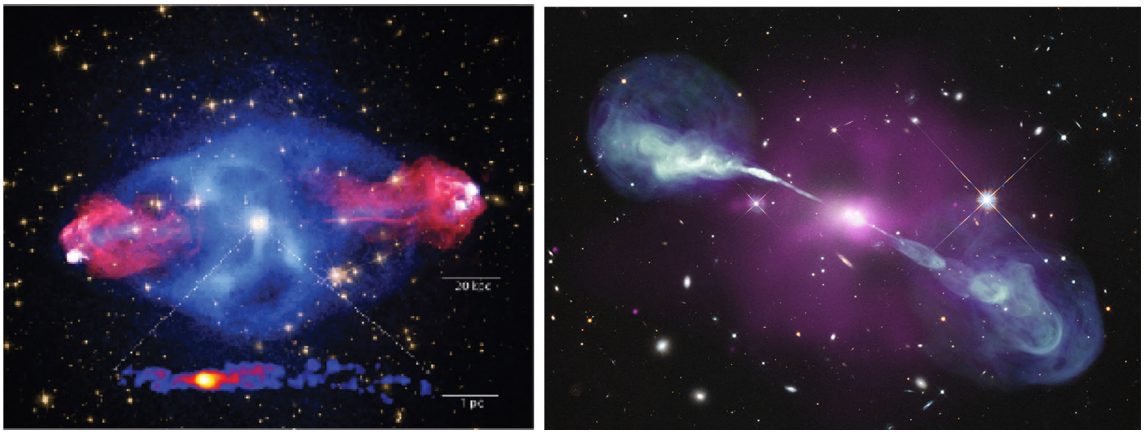

Figure 13. Left: Radio source Cygnus A shown in red, and hot gas emitting X-rays shown in blue; Right: Radio source Hercules A (in blue) with X-rays shown in purple. Radio and X-ray images are superposed on optical images from the Hubble Space Telescope of the galaxies and stars in the same field of view in both cases (Credits: Optical: NASA/STScI; Radio: NSF/NRAO/AUI/VLA; X-rays: NASA/HST/CXC/Columbia Univ./Johnson *et al.* (2019) for Cyg A; VLA/NASA/HST/CXC/SAO for Hercules A).

surface brightness of X-ray emission that encompass the radio lobes are known as cavities, and can be seen in both the images. Jets from powerful radio galaxies are thus capable of creating vast cavities by driving out gas. A large fraction of the energy is transferred by a jet and dissipated as thermal energy into the intra-galactic or intracluster hot gas. An example of such a cavity in a hot gas of a cluster of galaxies, Hydra A, is shown in Figure 14. Many examples of cavities have been reported to exist in many clusters of galaxies (e.g., one most recent example is in Abell (1569) reported by Tiwari & Singh (2022)). Kirkpatrick (2009) found that hot intracluster medium along the radio jets and lobes in Hydra A (Figure 14) is enriched with metals compared to that of the undisturbed gas. The enrichment extend covers a region with a radius of 20–120 kpc from the central galaxy transporting 20–70 million solar masses of iron out of the central galaxy (i.e., nearly 10–30% of the iron mass within the central galaxy) and uses only 1–5% of the total energetic output of central AGN, thus redistributing metal-enriched, low entropy gas throughout the core of the galaxy cluster (Kirkpatrick 2009). Similar enrichment has been reported by Million & Werner (2010) in M87 at radii between 350 and 400 arc-sec (27–31 kpc) from the AGN apparently in the wake of rising radio emitting bubbles carrying cool and metal-rich gas out of the central galaxy. They estimate that $\sim 1.0 \times 10^6$ solar masses of Fe could have been lifted and deposited at this distances, and that this mass is similar to the mass of Fe in the X-ray bright arms, suggesting that a single generation of buoyant radio bubbles may be responsible for the observed Fe excess.

Figure 14. Cluster of galaxies, Hydra A, in X-rays (blue) and radio (red) superposed on optical (yellow) image (Credits: X-ray: NASA/CXC/U.Waterloo/Kirkpatrick *et al.*; Radio: NSF/NRAO/VLA; Optical: Canada-France–Hawaii-Telescope/DSS).

4.2 *Feedback and regulation of star formation*

The above phenomenon is part of a process known as feedback from AGN into the cluster gas, and also plays a regulatory role in maintaining a balance between the cooling and heating in the cores of cluster gas and thus, the galaxy formation (Fabian 2012). Cores of many clusters of galaxies are known to have a radiative cooling time that is so short that a cooling 'flow' can be taking place thus, growing the mass of the central bright galaxies with the cooled gas

expected to lead to star formation (Fabian 1994). Evidence for the cooled gas and dust exists in the form of Hα nebulosities, molecular CO and H_2 gas, and infra-red emission observed in the cores of many clusters (and dominant elliptical galaxies in groups of galaxies), but there is little evidence for any vigorous star formation taking place in them. Several heating processes have been proposed which, can stop unhindered cooling flow. One of these is found to be heating by jets coming from the central SMBH, energy from which can heat the intergalactic gas and prevent the formation of large numbers of stars in a central galaxy (Fabian 2012).

Acknowledgements

The author thank the authors of many publications cited here for the use of images and graphs shown here. He also thank G. C. Dewangan and S. Chandra for the plots provided by them ahead of their publications. The author thank the organisers of the Workshop on 'Astrophysical jets and observational facilities: National perspective' held on 5–9 April 2021 at ARIES, Nainital, for inviting the author to speak on the subject title, and on which this article is based. He thank the Indian National Science Academy for support under the INSA Senior Scientist Programme.

References

Agrawal P. C., Riegler G. R. 1979, ApJL, 231, L25
Agudo I., *et al.* 2011, ApJ, 726, L13
Ajello M., Romani R. W., Gasparrini D., *et al.* 2014, ApJ, 780, 73
Beckmann V., Shrader C. R. 2012, Active Galactic Nuclei (Wiley-VCH Verlag GmbH: Weinheim)
Blazejowski M., Sikora M., Moderski R., Madejski G. M. 2000, ApJ, 545, 107
Boehringer H., Voges W., Fabian A. C., Edge A. C., Neumann D. M. 1993, MNRAS, 264, L25
Bottcher M. 2002, BASI, 30, 115
Bottcher M. 2007, Ap&SS, 309, 95
Bottcher M., Reimer A., Marscher A. P. 2009, ApJ, 703, 1168
Braun P. S. 2012. Adv. Space Res. 50, 96
Blandford R., Meier D., Readhead A. 2019, Annu. Rev. Astron. Astrophys., 57, 467. https://doi.org/10.1146/annurev-astro-081817-051948
Cao G., Wang J.-C. 2013, MNRAS, 436, 2170
Dermer C. D., Schlickeiser R. 1993, ApJ, 416, 458
Fabian A. C. 1994, Annu. Rev. Astron. Astrophys., 32, 277
Fabian A. C., Sanders J. S., Allen S. W., *et al.* 2003, MNRAS, 344, L43
Fabian A. C., Sanders J. C., Taylor G. B. 2006, MNRAS, 366, 417
Fabian A. C., Vasudevan R. V., Gandhi P. 2008, MNRAS, 385, L43
Fabian A. C. 2012, Annu. Rev. Astron. Astrophys., 50, 455
Ferrarese L., Merritt D. 2000, ApJ, 539, L9
Forman W., Jones C., Churazov I. E., *et al.* 2007, ApJ, 665, 1057
Fossati G., Maraschi L., Celotti A., *et al.* 1998, MNRAS 299, 433
Gasparyan S., Begue D., Sahakyan N. 2022, MNRAS, 509, 2102. https://doi.org/10.1093/mnras/stab2688
Graham J., Fabian A. C., Sanders J. S. 2008, MNRAS, 391, 1749
Hayashida M., Madejski G. M., Nalewajko K., *et al.* 2012, ApJ, 754, 114
Hazard C., Mackey M. B., Shimmins A. J. 1963, Nature, 197, 1037
IceCube Collaboration, *et al.* 2018a, Science, 361, 147. https://doi.org/10.1126/science.aat1378
Johnson A. C., *et al.* 2019, American Astronomical Society, AAS Meeting #233, id.243.16, bibcode: 2019AAS...23324316J
Kirkpatrick C. C., *et al.* 2009, ApJ, 707, L69
Kushwaha P., Sahayanathan S., Singh K. P. 2013, MNRAS, 433, 2380. https://doi.org/10.1093/mnras/stt904
Kushwaha P., Gupta A. C., Witta P. J., *et al.* 2018, MNRAS, 479, 1672
Mannheim K., Biermann P. L. 1992, A&A, 253, L21
Mannheim K. 1993, A&A, 269, 67
Maraschi L., Ghisellini G., Celotti A. 1992, ApJ Letters, 397, L5
Million E. T., Werner N., *et al.* 2010, MNRAS, 407, 2046. https://doi.org/10.1111/j.1365-2966.2010.17220.x
Mucke A., Protheroe R. J., Engel R., Rachen J. P., Stanev T. 2003, Astropart. Phys., 18, 593
Owen F. N., Eilek J. A., Keel W. C. 1990, ApJ, 362, 449
Schmidt M. 1963, Nature, 197, 1040
Shakura N. I., Sunyaev R. A. 1973, A&A, 24, 337
Seyfert C. K. 1943, ApJ, 97, 28
Shields G. A. 1999, PASP, 111, 661
Sikora M., Begelman M. C., Rees M. J. 1994, ApJ, 421, 153
Singh K. P., Tandon S. N., Agrawal P. C., *et al.* 2014, Proc. SPIE, Space Telescopes and Instrumentation 2014: Ultraviolet to Gamma Ray, 9144, 91441S. https://doi.org/10.1117/12.2062667
Singh K. P., Stewart G. C., Chandra S., *et al.* 2016, Proc. SPIE, in Space Telescopes and Instrumentation 2016: Ultraviolet to Gamma Ray, 9905, p. 99051E. https://doi.org/10.1117/12.2235309
Singh K. P., Stewart G. C., Westergaard N. J., *et al.* 2017, JApA, 38, 29

Singh K. P., Kushwaha P., Sinha A., Main Pal, Agarwal A., Dewangan G. C. 2022, MNRAS, 509, 2696. https://doi.org/10.1093/mnras/stab3161
Tadhunter C. 2016, Astron. Astrophys. Rev., 24, 10
Tandon S., Subramaniam A., Girish V., *et al.* 2017, AJ, 154, 128. https://doi.org/10.3847/1538-3881/aa8451
Tiwari J., Singh K. P. 2022, MNRAS, 509, 3321
Urry M. C., Padovani P. 1995, PASP, 107, 803
Wehrle A. E., *et al.* 1996, Blazar Continuum Variability, eds. Miller H. R., Webb J. R., Noble J. C., ASP Conference Series, Vol. 110, p. 430
Xue R., Liu R.-Y., *et al.* 2019, ApJ, 886, 23
Zhang J., Liang E.-W., Zhang S.-N., Bai J. M. 2012, ApJ, 752, 157